

---

## Chapter 6

# Thin Film Growth on Si(001)

### 6.1 Introduction

There are a few experimental results about growth of manganese films on Si(001) [15, 16, 128, 149]. They all agree in this point that pure Mn films can not be grown on these surfaces but hetero-structure Mn-Si compounds are observed. Wang *et al.* reported thin film formation of MnSi and  $\text{MnSi}_{1.7}$  at 400 and 600 °C by solid phase reaction on Si(001) [128]. Recently, in scanning tunneling microscope images, Lippitz *et al.* observed two different 3D-islands that were grown by deposition at around 450 °C. These islands are a pancakes-stack-like island which is interpreted as MnSi and a hut-like structure which seems to be  $\text{Mn}_5\text{Si}_3$ . The regular Si-dimer reconstruction with  $(2 \times 1)$  periodicity was also observed on the surface [16].

The Mn atoms in suitable chemical environments possess considerable magnetic moments. Moreover, both fcc-Mn and some MnSi compounds are closely lattice-matched with the Si(001) surface (within a few percent of the relevant lattice constants). Therefore, it is conceivable that Mn-silicide thin films could be grown on Si. It is interesting to discuss the stability of pseudomorphic Mn and MnSi thin films for growing ferromagnetic films on Si(001). The present work focuses on their atomic structure, thermodynamic stability, and magnetic properties.

It has been discussed in Chap. 2, that stable Mn bulk phases show either antiferromagnetic (AFM) ordering or complex spin structures [63], while the metastable ferromagnetic (FM) state emerges at an expanded volume. It is, therefore, conceivable that a ferromagnetic pseudomorphic fcc-Mn film, with a lattice constant slightly expanded to match the Si(001) surface, could be formed. Additional to such film the epitaxial structure of compounds is considered which is formally resulting from substitution of part of the Mn atoms in fcc-Mn by Si atoms. These films have locally a B2 structure of Mn-mono-silicide, which is not as stable as the

natural B20 structure but it can be grown epitaxially under non-equilibrium condition with molecular beam epitaxy (MBE) [76]. Recently, the stability of such films has been theoretically studied by Wu *et al* [150].

The stability of thin films containing more than 1 ML of Mn is conveniently discussed in terms of their formation energy. Since the Si dimer reconstruction is lifted already after deposition of 1/2 ML of Mn, it is appropriate to use a Si(001)-(1 × 1) unit cell to study thicker films.

The formation energy is defined as

$$E^{\text{form}} = \frac{1}{2}(E^{\text{tot}} - \sum_i N_i \mu_i) - \gamma_{\text{Si}(001)}^{\text{surf}} \quad (6.1)$$

where  $E_{\text{total}}$ ,  $N$  and  $\mu$  refer to the total energy per (1 × 1) supercell, the number of atoms in the (1 × 1) cell, and the chemical potential of the atomic species as calculated from bulk materials, respectively.  $\gamma_{\text{Si}(001)}^{\text{surf}}$  is the surface energy of the clean reconstructed Si(001) surface, which is found to be 1.25 eV per (1 × 1) cell in this work.

Since the ground-state  $\alpha$ -Mn has a complicated structure<sup>1</sup>, the total energy of  $\gamma$ -Mn has been calculated [63]. The chemical potential of Mn is obtained from our calculation for bulk Mn in the fcc-structure ( $\gamma$ -Mn) corrected by  $-0.07$  eV/Mn, which is the energy difference per atom between  $\alpha$ -Mn and  $\gamma$ -Mn.

All calculations in this chapter are done using a (1 × 1) supercell with a  $10 \times 10 \times 1$   $\mathbf{k}$ -point mesh for Brillouin zone integration.

In this section, two types of films are studied - either pure Mn or Mn-Si alloy films for up to 3 ML coverages are considered.

## 6.2 Coverage of 1ML on Si(001)

### 6.2.1 Thermodynamics, and Structural Stability

The foregoing calculations on Mn bulk established that the lattice constant for fcc-Mn is  $a=3.77 \text{ \AA}$ <sup>2</sup> which matches the Si(001)-(1×1) cell lattice of  $3.88 \text{ \AA}$  quite well. The atomic density of the Mn layer is twice that of a Si layer and therefore 2 Mn atoms per cell are considered as one monolayer for a Si(1×1) cell.

For 1ML coverage several growth possibilities are simulated. They can be divided

<sup>1</sup>See section 3.4 of chapter 3.

<sup>2</sup>the experimental value is  $3.72 \text{ \AA}$  [67].

into two categories, namely, i) a dense Mn layer and ii) a sparse Mn bilayer with a 1:1 ratio of Mn and substrate Si atoms. The structures and formation energies for both pure Mn and Mn-Si films in a ferromagnetic and an antiferromagnetic phase are summarized in fig. 6.1.

The formation energy for the first structure, formed by a dense Mn sub-layer with a Si-capping layer on top, is calculated, (Fig. 6.1-a). The presence of the Si-capping layer greatly reduces the energy costs for formation of a dense film on the surface. This is due to the higher coordination of Mn atoms in the sub-layer to Mn and Si neighbors, compared to a dense Mn overlayer. Putting the dense Mn layer on the surface, rather than in the sub-surface region, leads to an increase of the formation energy from 0.567 eV to 1.687 eV.

For the sub-layer Mn-film, the parallel spin alignment is found to be thermodynamically more stable than an intralayer anti-parallel spin arrangement, while a change from FM to AFM interlayer coupling is observed for an Mn film on the surface.

The capping-Si layer structure shows a strong buckling of 0.43 Å for Si and 0.17 Å for Mn, respectively. The bonding between Si atoms in the topmost layer and Mn atoms in the sub-layer is rather weak, leading to long Si<sub>2</sub>-Mn<sub>1</sub> and Si<sub>2</sub>-Mn<sub>2</sub> bonds (2.67 Å and 2.78 Å). These bonds are however essential for the stability of the structure. This can be seen by removing a Si<sub>2</sub> atom from the surface, which leads to an increase of the formation energy,  $E_{\text{form}}$ , of 0.77 eV.

The dense Mn layer with a Si-capped structure is also more stable than structures with mixed Mn-Si occupation. Four different structures for Mn-Si mixed phases are shown in Fig. 6.1(b, c, d, f). The AFM phase is considered as an interlayer structure of opposite spin orientation.

In the MnSi bilayer structure, 50% of the Mn atoms in the sub-surface layer are interchanged with atoms of the Si overlayer (cf. Fig. 6.1-b). Though this structure can be considered as a sparse alternating Mn-layer perpendicular to the surface, its formation energy still rises by the order of hundreds of meV compared to Mn in the sub-layer. Formation of an intralayer AFM spin alignment is more stable than both FM and interlayer AFM spin arrangement by 0.122 eV/unit cell and 0.129 eV/unit cell, respectively. In this structure the shortest interlayer distance in the Mn-Si bilayer is about 1.71 Å. This value is smaller than Mn in the overlayer and Mn in the sub-layer by 15 % and 20 % , respectively . Furthermore, the roughness and surface corrugation in this structure are reduced.

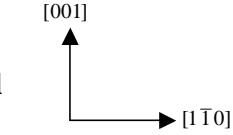
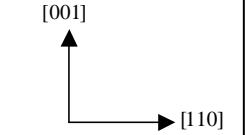
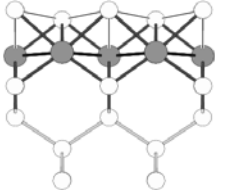
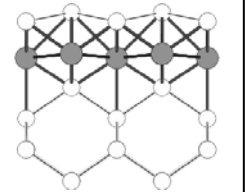
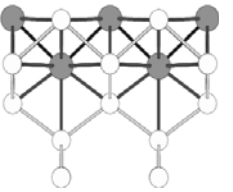
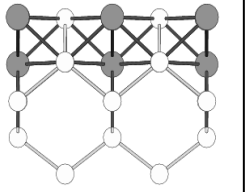
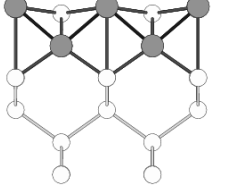
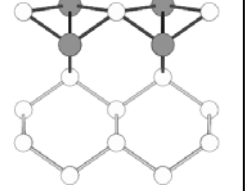
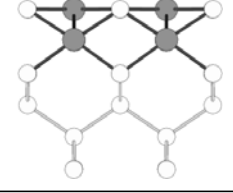
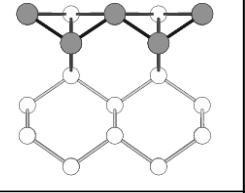
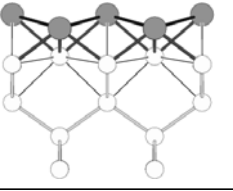
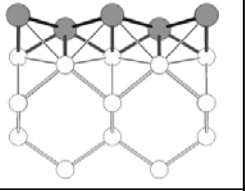
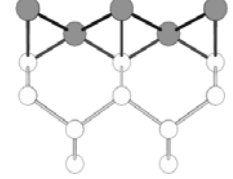
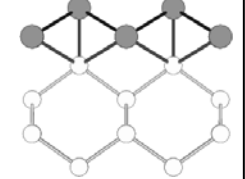
One ML Mn on Si(001)(1x1) cell			FM eV/cell	AFM eV/cell
<b>Dense layer Mn with capped Si</b> (a)  	0.567	0.787		
<b>Bilayer mixed Mn-Si</b> (b)  	0.902	0.895		
<b>Bilayer Mn-I</b> (c)  	1.399	1.435		
<b>Bilayer Mn-II</b> (d)  	1.471	1.446		
<b>Dense overlayer Mn</b> (e)  	1.704	1.687		
<b>Bilayer Mn-III</b> (f)  	2.56	2.37		

Fig. 6.1: Side view for two different directions of several configurations with 1 ML Mn coverage. Big black circles represent Mn and small white circles Si.

In addition, some other bilayer structures with

- i) One diluted Mn layer and one dense Mn-Si layer on top, Fig. 6.1-c, d and
- ii) Two diluted Mn overlayers, Fig. 6.1-f are considered.

In the later case, due to Mn-non-saturated bond and weak Mn-Mn bond is quite unstable and  $E_{\text{form}}$  in AFM phase is 2.37 eV. These results show that The adsorption in separate layers, i.e. one pure dense Mn monolayer is energetically more favorable than two intermixed layers.

The above allows the conclusion, that a Mn-dense layer with Si capping is the most stable structure (of the considered). For this reason we will concentrate on this arrangement of Mn and Si and study higher coverages of the dense atomic layer.

### 6.2.2 Electronic and Magnetic Structure

The different spin alignment between Mn-atoms in sub-layer and topmost layer was mentioned previously. Mn in the sub-layer has a ferromagnetic spin configuration, while the magnetic structure of Mn in the topmost layer is antiferromagnetic.

The origin of this magnetic transition, which is due to the structural transformation of Mn being moved from the topmost layer to the sub-surface layer, can be explained by an analysis of the orbital-projected density of states shown in Fig. 6.2.

In the Mn-DOS plots for both the overlayer and the sub-surface layer, a large exchange splitting<sup>3</sup> of almost 4 eV and 2 eV, respectively, is found. The  $d$ -band-widths of both the majority (minority) spin of Mn is narrower than in comparison to the bulk Mn which indicates the Mn- $d - d$  overlap is more than the Mn- $d$  and Si- $sp$  hybridization. The Mn  $3d$ -bands are broadened in the sub-layer structure and have a large overlap around the Fermi level, which reduces the spinpolarization at the Fermi level. The spin polarization ( $P$ ) of carriers is about 30 % at the Fermi level, as estimated from the spin-resolved total DOS shown in Fig. 6.2. The spin polarization is defined by:

$$P = \frac{\rho_{\uparrow}^{\text{F}} - \rho_{\downarrow}^{\text{F}}}{\rho_{\uparrow}^{\text{F}} + \rho_{\downarrow}^{\text{F}}} \times 100\% \quad (6.2)$$

where  $\rho_{\uparrow}^{\text{F}}$  and  $\rho_{\downarrow}^{\text{F}}$  are the density of states for spin up and down at the Fermi level, respectively.

According to the itinerant  $sp - d$  exchange model [151], in the Mn-Mn interaction two mechanisms are in competition over all interaction. These interactions can be

<sup>3</sup>The exchange splitting is measured by the difference between the position of the highest peak in the total DOS for spin up and spin down.

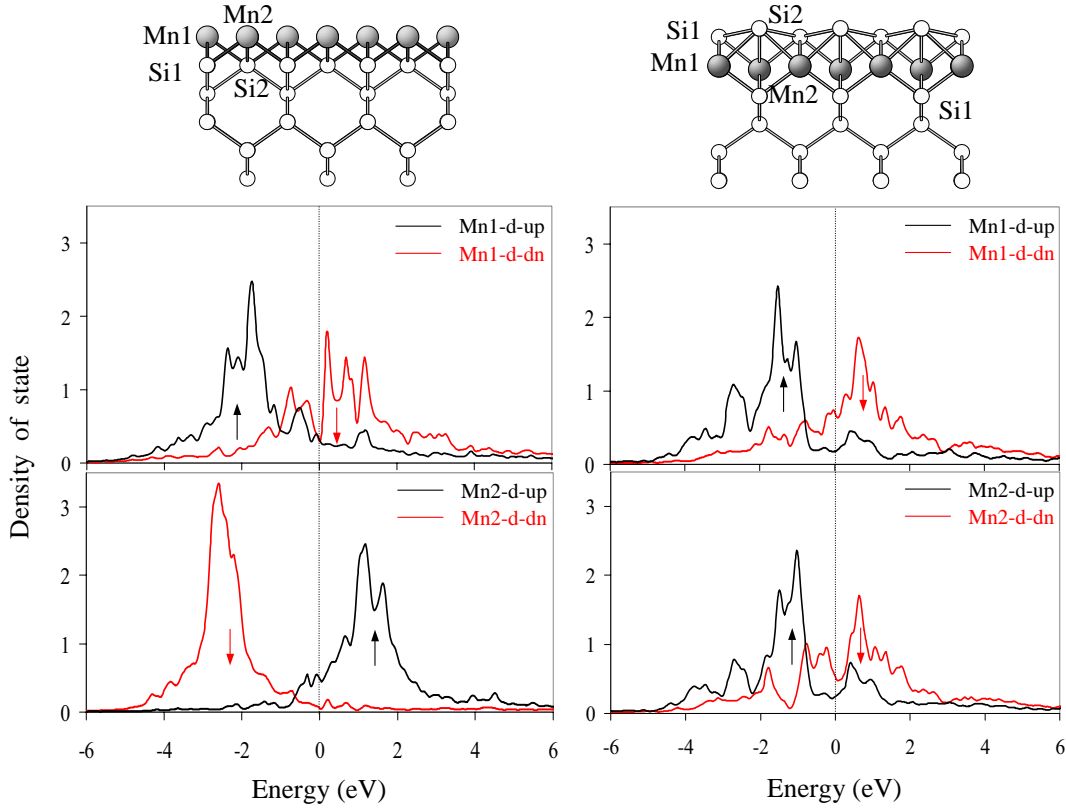


Fig. 6.2: Density of states for spin up and down  $d$ -orbitals of the Mn atoms in the a dense layer of the Mn-overlayer (left panel) and the Mn-sub-layer (right panel).

interpreted as the  $d-d$  direct antiferromagnetic coupling and the  $d-sp-d$  indirect interaction which the ferromagnetic coupling is more favorable.

There is AFM coupling between the Mn-sub-layer and its nearest neighbor Si. The Mn atoms interact with each other through the three Mn1-Si-Mn2 channels in the interface and capping layer. From itinerant  $sp-d$  exchange model, the electron kinetic energy can be reduced by itinerant  $sp-d$  exchange which this effect stabilizes the FM spin coupling between the Mn atoms [150].

The  $sp-d$  exchange in the Mn-overlayer is not as big as Mn-sub-layer because there is only one Mn1-Si-Mn2 channel. Then direct  $d-d$  exchange between Mn is more effective than the  $sp-d$  exchange between Mn and Si. This direct the  $d-d$  hopping makes an AFM Mn-Mn coupling. This is a qualitative explanation for the AFM-FM transition which is caused by the Si capping layer. Now the calculated results confirm this explanation also quantitatively. The Mn-sub-layer structure was found to have a FM ground state. The energy cost associated with a FM-AFM spin reverse is 0.22 eV/cell in the Mn-sub-layer which suggest that the  $sp-d$  exchange mediated FM coupling is rather strong in Si-Mn on Si(001).

The same justification is valid for Mn-Si bilayer (which is kind of double layer mixed) structure for which the intralayer AFM coupling has lower energy. In this atomic geometry, there are two hopping channels for itinerant electrons in the  $sp-d$  hybridized band but still the direct  $d-d$  exchange prevails effect, because the Mn-Mn distance is as short as the Mn-Si distances.

Table 6.1: Spin moments (in  $\mu_B$ ) of the Mn-overlayer, sub-layer and mixed MnSi layer at their respective magnetic ground states.  $Si^S$  is substrate atom,  $Si^I$  is an atom in the interface and  $Si^T$  is a Si-capping atom. Note that a non-negligible spin moment is induced on the Si atoms in surface and interface Mn.

Structure	$(Si)^S$	$Si_1^I$	$Si_2^I$	$Mn_1$	$Mn_2$	$Si_1^T$	$Si_2^T$
Mn-overlayer	-0.04	0.01	-0.042	-3.68	2.04	—	—
MnSi-bilayer*	0.03	—	0.00	-1.53	3.31	0.01	—
Mn-sub-layer	0.02	-0.07	—	1.61	2.16	-0.06	-0.04

(\*) refers to the Fig. 6.1-b

The lower coordination of Mn in the overlayer compared to the sub-layer increases the magnetic moments up to 40% from 2.16/1.61  $\mu_B$  for sub-layer to 3.67/2.04  $\mu_B$  for the topmost layer. The magnetic moments of the three top layer atoms in the discussed structures (shown in Fig. 6.1) are listed in Tab. 6.1. The induced magnetic moment in the Si atoms at the interface is larger than the one at the surface. Moreover, because of the strong Si-3 $sp$  Mn-3 $d$  hybridizations (also seen in Fig. 6.2), the Si 3 $p$  state becomes spin-polarized. The down-spin component below or at the Fermi level is increased compared to the up-spin component, and thus the two capping  $Si_1^T$  and  $Si_2^T$  and the interface  $Si_1^I$  have an induced negative spin moment.

Tab. 6.1 shows that the presence of a Si capping layer causes an interesting AFM-FM transition, thereby reducing the spin moment from 3.68  $\mu_B$  and 2.04  $\mu_B$  for Mn1 and Mn2 in the AFM structure to 2.16  $\mu_B$  and 1.61  $\mu_B$  for Mn1 and Mn2 in the FM Mn-sub-layer.

## 6.3 Coverage of 2ML on Si(001)

### 6.3.1 Thermodynamical and Structural Stability

The preceding discussion showed that a structure with a dense Mn layer covered by a Si layer is generally preferred over all others. This point supports further calculations with higher Mn coverage for only some probable structures. For  $\theta = 2$  ML

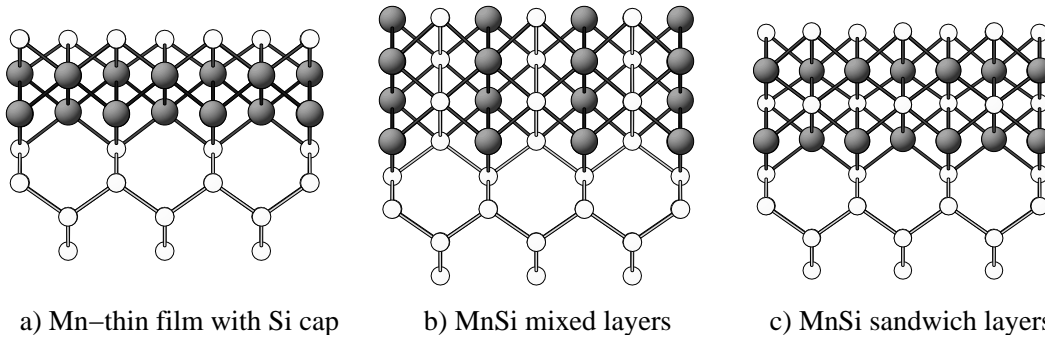


Fig. 6.3: Side view of structures with 2 ML coverage Mn/Si(001). Big black circles represent Mn atoms and small white circles represent Si atoms.

three structures with a FM, an interlayer AFM and an intralayer AFM magnetic configuration are studied (see Fig. 6.3):

- 1) A structure with a pure Mn-thin film and Si in the topmost layer.
- 2) A mixed MnSi layer structure with an 1:1 ratio of Mn and Si. The Mn and Si layers are alternating perpendicular to the surface. The atomic arrangements in this structure resembles the atomic positions in a [100] plane of the cesium chloride structure.

- 3) A sandwich MnSi layer structure with alternating Mn and Si layers in the [001] plane and a resolved Si-overlayer. This structure resembles the CsCl structure in direction parallel to the surface.

The most stable film is the MnSi sandwich with a negative  $E_{\text{form}}$ , which indicates that the film is stable relative to decomposition into a clean silicon surface and bulk manganese. In Tab. 6.2, the calculated  $E_{\text{form}}$  in eV and the vertical interlayer distances in Å for all structures are shown.

In view of the strong (weak) intralayer (interlayer) FM coupling of the Mn layers in the above mentioned sandwich structures, the structures with  $\geq 2$  ML Mn coverage are modeled by i) FM coupling ( $\uparrow\uparrow\uparrow$ ), ii) intra-layer FM and interlayer AFM coupling and iii) intra-layer AFM but inter-layer FM ( $\uparrow\downarrow\uparrow$ ) coupling.

The formation energy of the FM B2(001) structure is -0.507 eV, which is lower than both the AFM Mn-thin film and the MnSi film by more than 1 eV. In this structure Mn atoms at the interface have six (or seven) bonds with Si while Mn atoms in the inner layers are eightfold coordinated. The surface roughness at this coverage is reduced in comparison to similar structures with 1 ML Mn coverage and the average vertical distance between layers decreases from 1.7 Å at 1 ML coverage to 1.4 Å and 1.6 Å at 2 ML<sup>4</sup>. Therefore, from thermodynamic stability considerations

<sup>4</sup>These are the distances between layers from the interface to the surface.



Table 6.2: Formation energy (eV/cell) for different magnetic ordering and interlayer distances (Å) for the three structures with 2 ML coverage, shown in Fig. 6.3.

Structure	FM	Interlayer AFM	Intralayer AFM	Intralayer distance(Å)
	Pure Mn with Si cap	—	0.53*	1.27
B2(001) film (mix)	0.528	0.726	0.85	1.4/1.7
B2(001) film (sandwich)	-0.507	-0.444	-0.164	1.4/1.6

(\*) Reference [150]

and structure analysis, it follows that bonds in thicker layers are stronger and the structures become more stable.

The formation energy for a Mn-thin film and B2(001) film, shown in the Tab. 6.2, are positive. The average interlayer distances are 1.4 Å for the interface,  $\sim 1.6 \pm 0.03$  Å for the inner layers and 1.7 Å for the surface. It is not sensitive to the thickness of the film in the B2(001) structure.

The results for the pure Mn film are just for the AFM phase, because self-consistent calculations did not support FM structures.

### 6.3.2 Magnetic Structure

The B2(001) structure has a FM metallic ground state with total spin polarization of about 50% at the Fermi level.

The interfacial-layer Mn atoms with sixfold (or sevenfold) coordination have an averaged magnetic moment of  $1.90 \mu_B$ /layer. This value is the same as for the previously described ground state of this structure at 1 ML coverage. Due to the higher coordination of Mn atoms in the inner layer (eightfold coordination), the averaged magnetic moment is decreased to  $1.11 \mu_B$ /layer. The *sp-d* hybridizations induce an averaged magnetic moment of 0.02, -0.07 and -0.04  $\mu_B$  at the Si atoms in the capping-layer, the middle layer and the first layer of the substrate, respectively.

Note that the *sp-d* exchange mediated FM intralayer coupling is as strong as for the same structure at 1 ML coverage. The energy cost to orient the magnetic moment of the Mn atoms within two layers in opposite directions (interlayer AFM) is 16 meV/Mn and to reverse it from parallel to antiparallel for Mn atoms in the same layer (intralayer AFM) is 86 meV/Mn<sup>5</sup>.

Within the layer, the indirect *d-sp-d* coupling between Mn atoms is stronger than direct *d-d* coupling, because within the two dimensional layer the itinerant *sp-d* hy-

<sup>5</sup>At coverage of 2 ML there are four Mn atoms in the unit cell.

bridized electrons mediate laterally between Mn atoms in the layer. On the other hand, the  $d-d$  coupling has dominant effect between Mn atoms in the subsequent layers. The formation energy indicates that, the FM interlayer coupling is weaker than the intralayer FM coupling. Therefore, one can conclude that  $d-sp-d$  coupling is always stronger than  $d-d$  coupling between Mn atoms. Additionally, the distances between Mn atoms play role for changing magnetic structure.

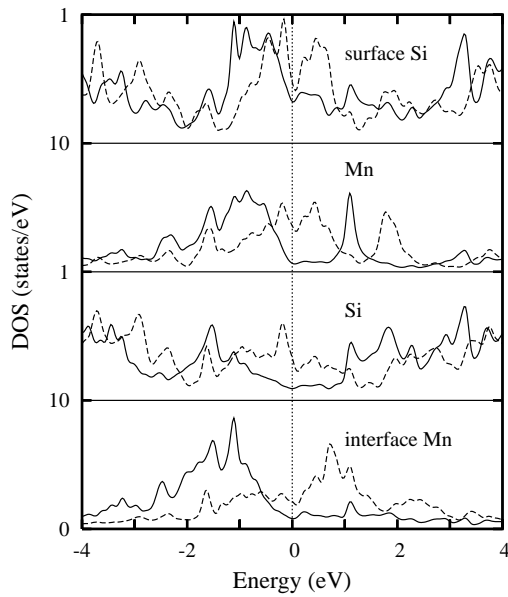


Fig. 6.4: The overlayer-resolved DOS of the FM 2(Si-Mn)/Si(001) film. The overlayers are shown from surface (top) to interface (bottom). Full lines show the majority spin, dashed lines the minority spin component. The considerable spin polarization of carriers at Fermi level (zero energy) is evident.

structure. In particular, the interface Mn layer has a spin polarization of up to 45%. These findings make the ultrathin B2(001) films interesting candidates in the search for spintronic materials [152].

The nearest intralayer Mn-Mn distance is about 2.74 Å which is shorter than the Mn-Mn in-plane distance by 0.26 Å.

For pure Mn thin films, the Mn atoms on the surface have the large average magnetic moment of about  $-3.2 \mu_B/\text{Mn}$  due to the presence of the surface, while the spin moment of the interface Mn atoms is reduced to  $1.5 \mu_B$ . The magnetic moment of a Mn atom with sixfold coordinations is bigger than for a Mn with sevenfold coordination, because the bond-lengths are shorter for the sevenfold coordination.

At one monolayer coverage the interlayer AFM magnetic structure has lower formation energy, whereas  $E_{\text{form}}$  at 2 ML coverage for the FM state is lower than for the AFM state by  $0.062 \text{ eV}/\text{Mn}$ .

Fig. 6.4 shows the overlayer resolved density of states of the 2 ML B2(001)

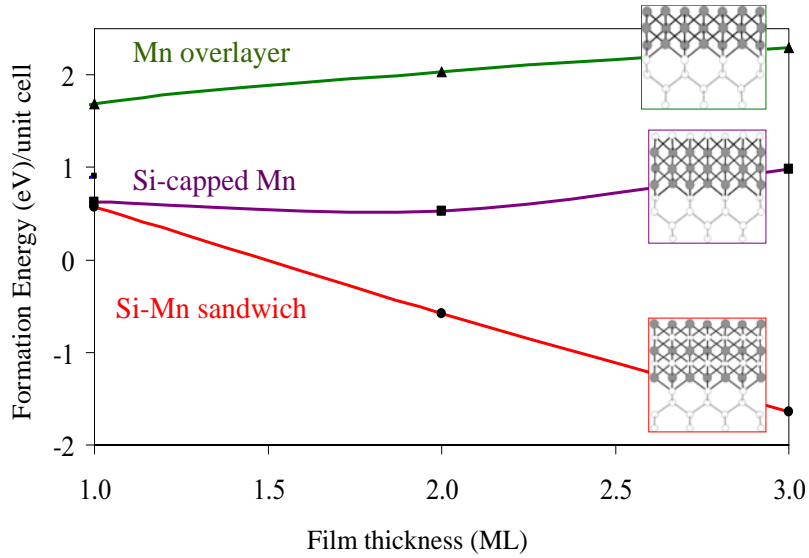


Fig. 6.5: Formation energy of pure Mn films and MnSi films in the B2(001) structure as a function of the film thickness. The zero of the energy scale refers to the surface energy of the clean reconstructed Si(001) surface. The green line corresponds to the pure Mn overlayer-film, the purple line corresponds to the Mn thin film with a Si capping layer and the red line to the MnSi sandwich film in the B2(001) structure.

## 6.4 Coverage of 3ML on Si(001)

### 6.4.1 Thermodynamical and Structural Stability

In order to find a common rule for the stability of film formation, the calculations for the B2 structure (sandwich Mn-Si film) and the pure Mn film are repeated for 3 ML Mn coverage [150, 152].

At  $\theta = 3\text{ML}$ , the most stable structure is the MnSi sandwich layers which has negative formation energy. The 3 ML B2(001) on Si(001) has a Mn-Si interlayer distance of 1.46 Å, 1.40 Å and 1.48 Å for the inner, middle and outer Mn layers, respectively. The Mn film is found to be highly strained and the average Mn-Mn nearest distance in the layer is 2.74 Å and thereby longer than the Mn bulk value in the ground state<sup>6</sup> by almost 8%.

In Fig 6.5, the stability of films formation is shown as a function of film thickness. As we have found earlier [150], a film with a B2 structure of alternating Mn and Si layers, terminated by a Si layer, has the lowest energy of all investigated candidate structures. In particular, it is much more stable than a film of pure Mn (filled trian-

<sup>6</sup>The nearest Mn-Mn distance in fcc structure in the ground state (AFM phase) is 2.54 Å and in the FM state 2.67 Å.

gles in Fig. 6.5), or a film of Mn capped by a Si monolayer (filled squares in Fig. 6.5). These findings can be rationalized by the fact that Mn–Si bonds are stronger than the average of Mn–Mn and Si–Si bonds; hence the system tends to maximize the number of Mn–Si bonds. In the sandwich films, the local coordination of a Mn atom is similar to the bonding in the cesium chloride (CsCl) crystal structure, i.e., each Mn atoms has eight Si neighbors. However, due to epitaxial strain, the local environment of a Mn atom does not have cubic symmetry, but is slightly distorted, and Mn–Si bond lengths vary by several percent within the film, being shortest in its interior and longer near the surface and interface. Negative values of  $E_{\text{form}}$  in Fig. 6.5 indicate that the film is thermodynamically stable with respect to decomposition into a clean Si surface and bulk Mn metal. This is the case for films formed by depositing 2 ML of Mn or more.

#### 6.4.2 Electronic and Magnetic Structure

In all magnetic structures of MnSi film, the magnetic moment of the central Mn layer almost vanishes (the calculated averaged spin moment is only about  $0.1 \mu_B/\text{Mn}$ ).

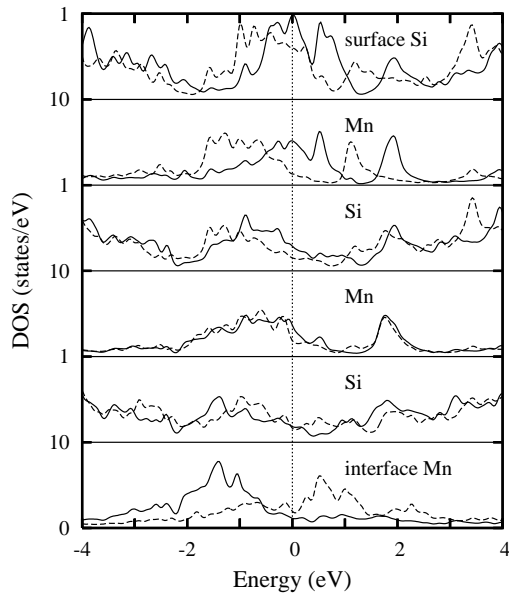


Fig. 6.6: The overlayer-resolved DOS of the interlayered AFM 3(Si-Mn)/Si(001) film. See Fig. 6.4 for other notes.

The lack of magnetic moment in the central layer is due to strong Mn-3*d* and Si-3*sp* hybridizations which is caused by eight coordinations of Mn atom with Si and also the shortest Mn-Si interlayer distance of 1.40 Å. The intralayer distance is slightly elongated in comparison to interlayer distances of 1.46 Å for both the inner and outer Mn layers. All these interlayer distances are shorter than the one between Mn layers in the 1 ML Mn-Si structure and the interface (surface) Mn layer in the 2 ML Mn-Si. It is therefore not surprising that in the 3 ML sandwich Mn-Si structure, the spin moment of the interface (surface) Mn layer is reduced to  $1.72$  ( $0.91$ )  $\mu_B$ .

In addition, the induced spin moment of the sandwich-layer Si decreases to  $-0.03 \mu_B$ .

Moreover, the magnetic state with interlayer AFM coupling between the interface and surface Mn layers in the 3 ML B2(001) structure on Si(001) is calculated. It is found that besides the almost vanishing spin magnetic moment of the central Mn layer ( $-0.15 \mu_B$ ), the spin moment is  $1.75$  ( $-1.07$ )  $\mu_B$  for the interface (surface) layer Mn. This interlayer AFM structure has a little lower negative  $E_{\text{form}}$  of  $-1.53$  eV and is the magnetic ground state. Note that the surface and interface of the 3 ML sandwich thin film can be regarded as a antiferromagnet (film) with a central magnetically dead layer.

For the 3 ML B2 structure, it is found that the surface and interface Mn layers are magnetically active, while the middle Mn layer becomes nearly nonmagnetic. This can be attributed to a stronger covalent bond between Mn and Si in the middle layer, which is indicated by the shorter Mn-Si bond length.

In contrast to the weak FM interlayer coupling in the 2 ML sandwich mentioned above, the 3 ML sandwich Mn-Si film shows an energetic preference for the magnetic moments of the surface Mn atoms and the interface Mn atoms to point in opposite directions. This AFM interlayer (structure B in Fig. 6.7) is lower in energy than the FM state and the nonmagnetic one by 15 and 120 meV/Mn, respectively [150]. Note, however, that the FM intralayer coupling persists also in the 3 ML B2(001) structure.

The AFM interlayer coupling (structure B in Fig. 6.7) between the interface and surface Mn layers is partly due to the almost vanishing but antiparallel spin moment of the middle Mn layer (to the interface Mn layer) with the smallest interlayer spacing and the strongest Mn-Si covalency. In a sense, such an AFM coupling could, via the almost non-magnetic intermediate Si-Mn-Si trilayer complex, have a superexchange origin. Furthermore, it follows that energy difference between parallel and antiparallel alignment of spin magnetic moment on neighboring in-layer Mn atoms is about 82 meV/Mn (see structure (A) and (C) in Fig. 6.7). This indicates once again the strong FM intralayer coupling in these sandwich films.

The spin moment of the middle-layer Mn in the 3 ML pure Mn/Si(001) structure, being around  $1 \mu_B$ , is smaller than the calculated bulk-phase value of  $1.9 \mu_B$ . This is not surprising, since the Mn film is found to be highly strained and the middle-layer averaged Mn-Mn nearest distance of  $2.48 \text{ \AA}$  is shorter than the bulk value of

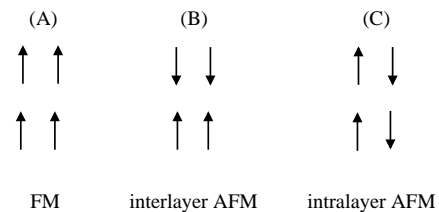


Fig. 6.7: Ferromagnetic (A), interlayer antiferromagnetic (B) and intralayer antiferromagnetic (C) structure of B2(001)/Si(001).

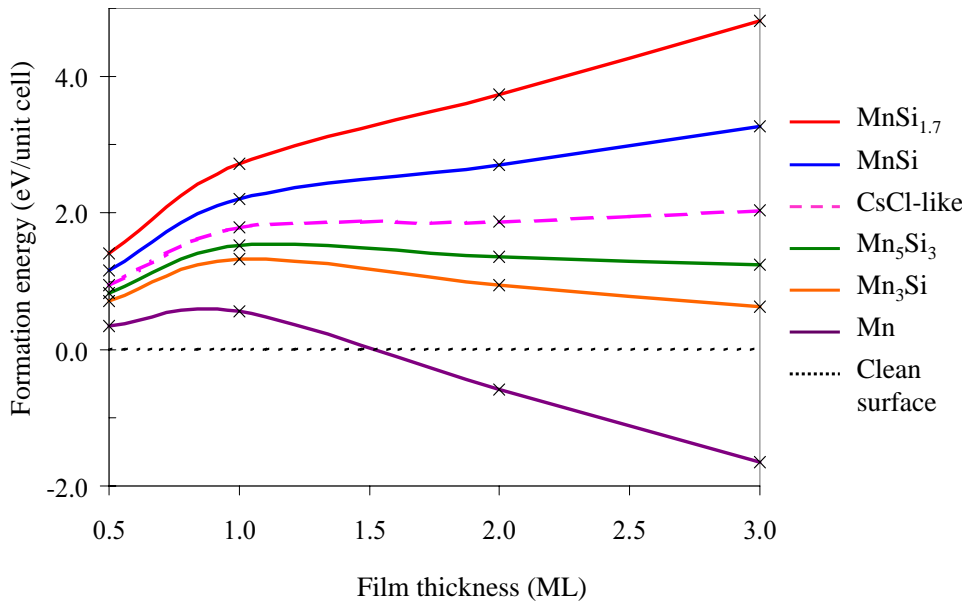


Fig. 6.8: Formation of films with B2 structure of Mn-mono-silicide on Si(001) in equilibrium with some Mn-silicide structures. The surface energy of the clean (001) reconstructed surface is considered as zero point. Formation of these films on the surface is unstable in equilibrium with Mn-poor compounds.

2.54 Å .

Fig. 6.6 provides the DOS plot for the 3 (Si-Mn)/Si(001) sandwich. It is evident that both the Mn and Si overlayers have a considerable spin polarization of carriers at the Fermi level, as we reported earlier for (Si-Mn)/Si(001) [150]. In particular, the interfacial Mn layer has a spin polarization of up to 27% in the 3 (Si-Mn)/Si(001) sandwiches.

It is therefore concluded that the growth of Mn overlayers on the Si(001) surface is energetically rather unfavorable. The pure Mn films on Si(001) is unstable and it turns into the Mn-Si sandwich structures.

## 6.5 The Thermodynamic Stability

Most of the experiments indicate that Mn prefers to form a silicide when grown on Si surfaces. In 1985 the epitaxial growth of (001)MnSi<sub>1.7</sub>/Si(001) was reported by Lian *et al.* [15] and recently, Lippitz *et al.* observed that, MnSi and Mn<sub>5</sub>Si<sub>3</sub> islands could be formed [16] . Also it was discovered by molecular beam epitaxy (MBE) that, some transition metal mono-silicides <sup>7</sup> ( CoSi, FeSi) can be crystallized in the

<sup>7</sup>These intermetallic compounds are isostructure with four Mn and Four Si atoms in a simple cubic structure with space group  $P2_13$  and pearson symbol  $cP8$ .

CsCl structure on Si surfaces [76]. Moreover, among the known bulk phases of Mn silicides,  $\text{Mn}_3\text{Si}$  in the  $\text{D0}_3$  structure appears to be compatible with pseudomorphic thin film growth on  $\text{Si}(001)$ <sup>8</sup>, but (as bulk compound) is known to be only weakly magnetic [154]. These results motivate us to calculate the film stability of the proposed structures in equilibrium with known Mn-silicide structures in this surface.

From the curves in Fig. 6.8, the sandwich films with CsCl structure are metastable relative to the Si-rich compounds (bulk MnSi or  $\text{MnSi}_{1.7}$ ). The formation of a pseudomorphic CsCl-like structure is endothermic in equilibrium with bulk MnSi and  $\text{MnSi}_{1.7}$ . In contrast, film formation in equilibrium with Mn-rich compounds (or bulk Mn) are exothermic and become stable for thicker films. The negative  $E_{\text{form}}$  shows that multilayers [ $n(\text{Si-Mn})/\text{Si}(001)$ ] are thermodynamically stable against decomposition into the elements for  $n \geq 2$ . Note that in this curve, the formation energy of the CsCl-like films,  $E_{\text{form}}(\theta)$ , decreases almost linearly with film thickness in the regime of multilayer-films. The almost linear decrease between 1 ML and 3 ML indicates that the interior of a 2–3 ML thick film has already properties similar to those of bulk MnSi in the CsCl structure.

However, as a consequence of the negative curvature, at small thickness a thin homogeneous film is unstable against decomposition into a thicker film that only partly covers the surface, plus a corresponding area of clean  $\text{Si}(001)$ <sup>9</sup>.

We stress that the deposition of Mn on Si does *not* lead to the formation of a wetting layer, because the formation energy of thin films ( $\leq 2$  ML) is higher than that of the clean  $\text{Si}(001)$  surface. Moreover, a homogeneous film is less stable than three-dimensional islands on clean  $\text{Si}(001)$ , see Sec. 7.7.1. Thus, MnSi on  $\text{Si}(001)$  is expected to grow in the Volmer-Weber growth mode. Since it is plausible that parts of the  $\text{Si}(001)$  surface remain uncovered, these surface areas can act as a continuous source for Si that feeds to growing MnSi islands during further deposition of Mn.

Moreover, it leads to the conclusion that interface growth depends very much on the substrate preparation: From our calculations, it is apparent that Mn adatoms bind very strongly to missing-dimer defects (and probably others defects and steps) on the  $\text{Si}(001)$  surface. We speculate that these binding sites, if present, could act as very efficient nucleation centers for three-dimensional island growth on MnSi. Only in the absence of these nucleation centers, two-dimensional film growth appears to be possible. Similar observations of a preparation-dependent interface growth were made in experiments of Co silicide formation on  $\text{Si}(001)$ . [155]

<sup>8</sup>For  $\text{Fe}_3\text{Si}$ , this structure was inferred from LEED analysis, see Ref. [153].

<sup>9</sup>More details about conditions for island formation are given in chapter 7

